PCCP

Accepted Manuscript

ROYAL SOCIETY OF CHEMISTRY

www.rsc.org/pccp

N, F-Monodoping and N/F-Codoping Effects on the Electronic Structures and Optical Performances of Zn_2GeO_4

Yulu Li,[a] Kaining Ding,*[a] Beisi Cheng,[a] Yongfan Zhang,[a,b] and Yunpeng Lu[c]

[a] *Department of Chemistry, Research Institute of Photocatalysis, State Key Laboratory of Photocatalysis on Energy and Environment, Fuzhou University, Fuzhou, Fujian, 350108, China*

[b] *Key Laboratory of Optoelectronic Materials Chemistry and Physics, Chinese Academy of Sciences, Fuzhou, Fujian, 350002, China*

[c] *Division of Chemistry and Biological Chemistry, School of Physical and Mathematical Sciences, Nanyang Technological University, 21 Nanyang Link, Singapore, 637371, Singapore*

** To whom correspondence should be addressed. Email: dknfzu@fzu.edu.cn; Tel: +83-0591-2866154*

Abstract

First-principles density-functional calculation has been performed to investigate the synergistic effects of N and F doping on the photocatalytic properties of Zn_2GeO_4. Our results indicate that with the presence of F facilitate the introduction of N by reducing the formation energy significantly. As N and F is codiping into Zn_2GeO_4, the mobility of the charge carriers is more rapidly due to the dispersive levels above the valence band. And with the narrowed band gap the optical absorption spectrum red-shift into the ideal visible-light region. Thus, we propose that the codoping of N and F can be a promising strategy to promote the photocatalytic performances of Zn_2GeO_4 under visible light.

1. Introduction

Since Fujishima and Honda demonstrated that crystalline TiO_2 could split water into H_2 and O_2, photocatalysts have drawn great attention in both industrial and scientific communities due to their potential applications in energy and environmental related fields, such as hydrogen production and water purification[1, 2]. Over the past decades, many semiconductors[3, 4] from the modified-TiO_2 to non-TiO_2 based semiconductor materials have been used as photocatalyst, while the efficiency of photoelectrochemical(PEC) water-splitting under visible-light irradiation is still low and far from practical application. The major obstacle to progress in this field is the lack of ideal semiconductor photocatalyst that satisfy the following requirements[5-8], (1) appropriate band gap (1.6–2.2 eV) for efficient visible light absorption; (2) high carrier mobility; (3) suitable band edge positions that straddle the water redox potentials; (4) chemical stability to corrosion and photocorrosion in aqueous environments. Therefore, engineering efficient photocatalyst are of great significances with some challenges.

To date, many of the explorations of the effective photocatalyst focus on the metal oxides containing d^0-transition metal cations(e.g., Ti^{4+}, Zr^{4+}, Nb^{5+}, Ta^{5+}, and W^{6+})[9] or d^{10}-typical metal cations (e.g., Ga^{3+}, In^{3+}, Ge^{4+}, Sn^{4+}, and Sb^{5+})[10], and principal metal compounds such as indates ($CaIn_2O_4$,$SrIn_2O_4$, $NaInO_2$, $LaInO_3$)[11], zinc gallate($ZnGa_2O_4$)[12, 13], strontium stannate(Sr_2SnO_4)[14], and various antimonates ($Ca_2Sb_2O_7$, $SrSb_2O_7$), $CaSb_2O_6$, $NaSbO_3$)[15]. Zinc germanate (Zn_2GeO_4) as an important p-block metal oxides with d^{10} configuration is not only a sort of glass or ceramic having special optical properties but also an efficient photocatalyst. Sato[16] et al. found that RuO_2-dispersed Zn_2GeO_4 has excellent activity for overall water splitting reaction. The photocatalytic activity of Pt-RuO_2/Zn_2GeO_4 for water splitting is 2.2 times of Pt /Zn_2GeO_4 and 3.3 times of RuO_2/Zn_2GeO_4 reported by Li et al.[17]. Zou et al.[18] prepared zinc orthogermanate by hydrothermal method and confirmed its perfect photocatalytic activity for water splitting and reduction of CO_2. A multiple-metal oxide Ag_2ZnGeO_4[19] with an indirect band gap(2.29 eV) shows

excellent catalytic ability for Rhodamine B and Orange II photodegradation in aqueous phase under visible-light irradiation. Unfortunately, because of its wide band gap (about 4.50 eV)[18, 20], pure Zn_2GeO_4 bulk only response to UV-light, which greatly restricts its photocatalytic efficiency and practical applications. A big concern is how to extend the optical absorption is significant for improving the photocatalytic activity of Zn_2GeO_4 in the ideal visible-light region.

It is well known doping foreign elements has become one of the primary strategies for modulating the electronic structure of semiconductors, which will affect their absorption behavior. For instance, nonmetal-doped TiO_2 exhibits higher thermodynamic stability and less recombination centers of charge-carries[21-23]. Up to now, nitrogen has been extensively applied for the energy band engineering of TiO_2, which shows remarkable red shifts of the absorption edges[24, 25]. A lot of investigations on the fluorine doped photocatalyst with narrowed band gap have been reported, such as F-doped TiO_2[26-30], $ZnWO_4$[31], SnO_2[32]. Although doping effects are actually receiving noticeable attention, doping is not a guarantee of successful efficient visible photocatalyst. This is due to that single element doping with wide band gap semiconductor has some shortages[13] such as a desirable dopant has limited solubility, and even if the desirable dopant has sufficient solubility, it may produce levels that are not located in the band gap, and in some cases spontaneous formation of compensating defects, et al. A new donor–acceptor codoping concept was proposed to improve the performance of a photocatalyst because donor-acceptor pairs codoping can reduce charged defects and then alter the electronic structure-dependent properties. (Ta, N)[33,] Nb/N-[33], Sb/N-[34], and Cr/N-codoped[35] TiO_2 have been prepared with good modified activity for water splitting under visible light. Theoretically, the modified mechanism of N/W-codoped[36], Mo/Zn-codoped[37], F/Zr-codoped[30] TiO_2 has been demonstrated by Run Long et al. In addition, nonmetal pairs doping researches also made some achievements [38-44]. On the new non-Ti semiconductor materials, some experimental results proposed that ZnGe oxynitride[45, 46] can photocatalytically oxidize organic pollutants with visible light irradiation indicating that elements implanting may affect the electronic state and optical properties of Zn_2GeO_4. However, to our

best knowledge, up to date, there are no direct researches on the doping modification of Zn_2GeO_4 to modulate its electronic structure and optical properties. Thus, it is valuable to research on this direction.

Enlightened by the success in the aforementioned examples, we attempt to examine the electronic structure of Zn_2GeO_4 by element doping effects to improve the catalytic performance under visible light irradiation. In the present work, N and F are chosen as the dopants to substitute O. A comprehensive theoretic study were carried out to reveal the N, F doping effects on the geometries and electronic structures of Zn_2GeO_4 based on DFT.

2. Models and Computational Methods

First-principle DFT calculations were performed by the Cambridge Serial Total Energy Package (CASTEP) code[47]. The generalized gradient approximation (GGA/PBE[48]) was adopted to optimize the crystalline cells and the atomic positions of pure and doped Zn_2GeO_4 compounds. In order to decide appropriate method to research the electronic states for these systems, standard DFT(GGA/PBE, LDA/CA-PZ[49]) and hybrid DFT(HSE06[50], and PBE0[51, 52]) were employed to calculate the band gap of the undoped Zn_2GeO_4. With the standard DFT, the kinetic cut-off energy for the plane-wave expansion was set to 420 eV and the ion-electron interactions were modeled by the ultrasoft pseudopotential with the Vanderbilt form[53]. While 750 eV and norm conserving pseudopotential were set for the hybrid DFT calculations, respectively. The valence atomic configurations were $3d^{10}4s^2$ for Zn, $4s^24p^2$ for Ge, $2s^22p^4$ for O, $2s^22p^3$ for N, and $2s^22p^5$ for F, respectively. The sizes of the Monkhorst–Pack k-point meshes were set as $2\times2\times2$, and the SCF tolerance was set to 2.0×10^{-6} eV/atom. In view of the accurate electronic properties of the pure system from different functionals, the PBE0 method was adopted to calculate the electronic structures of the N-doped, F-doped and N/F-codoped Zn_2GeO_4 with the same convergence parameters as applied in the pure Zn_2GeO_4, and the effects of spin polarization were considered. As displayed in Figure 1, the pure Zn_2GeO_4 is

constituted by GeO_4 and two types of ZnO_4 tetrahedrons. In our models, the conventional cell of pure Zn_2GeO_4 bulk that contains 6 Ge atoms, 12 Zn atoms and 24 O atoms (namely, 6 Zn_2GeO_4 units) was employed, and according to the coordination environment, the 24 O atoms can be divided into four types and denoted as O_a, O_b, O_c and O_d (Figure 1), respectively. Therefore, four different substitutional sites were considered, and by comparing the total energies of different doping models our results indicated that the N and F dopants tend to replace the oxygen at the O_c site (Figure 2a). For the N/F-codoped systems, we also considered all possible doping sites and the most stable structure was shown in Figure 2b. For the single N, F-doped systems, the doping concentration was 2.38% based on the 42 atom in the host cell, and the stoichiometries were $Zn_2GeO_{3.83}N_{0.17}$, and $Zn_2GeO_{3.83}N_{0.17}$, respectively. For the N/F-codoped system that N and F atoms replace two O_c atoms simultaneously, the stoichiometric expression is $Zn_2GeO_{3.67}N_{0.17}F_{0.17}$.

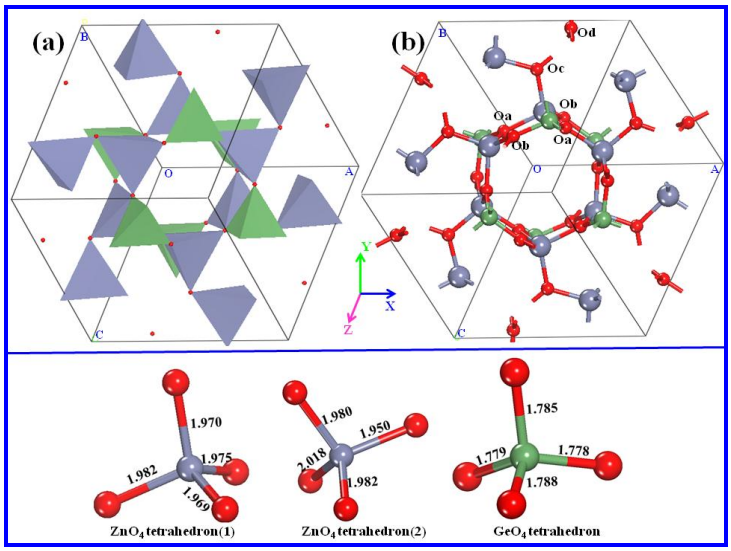

Fig. 1: The conventional cell for the hexagonal crystal structure for Zn_2GeO_4, (a) for polyhedron configuration, (b) for the ball and stick configuration. The lattice sites for the oxygen are indicated by Oa, Ob, Oc, and Od. The red, gray and green balls are O, Zn, and Ge atoms, respectively.

3. Results and Discussions

3.1 Geometry Structures and Thermodynamic Stability

The pure Zn_2GeO_4 belongs to a typical willemite structure with rhombohedral cells (a=0.8839 nm and R=107.79 °)[16]. The atoms are arranged in layers at six equally separated levels along the *c* axis, and each of Ge and Zn ion is in a tetrahedral

environment of four oxygen atoms as shown in Figure 1. One GeO_4 tetrahedron and two kinds of ZnO_4 tetrahedrons are combined each other through the edge oxygen atoms. The different Ge-O and Zn-O bonds in polyhedrons indicate that the GeO_4 and ZnO_4 tetrahedrons are distorted, which is in line with the experimental results. In the optimized structure of N-doped Zn_2GeO_4 displayed in Figure 2, the introduced N atom bonds to one Ge and two Zn atoms with little impacts on the bonds in the crystal cells. As listed in Table 1, the N-doped system has a slight increase of the volume compared with pure Zn_2GeO_4 bulk, which may due to the larger atomic radius of N (0.70 Å) than that of O (0.66 Å). In addition, the GeO_4 and ZnO_4 around the ZnO_3N tetrahedrons hardly suffer from distortion, illuminating that N-doping in Zn_2GeO_4 introduces a relative small local geometric distortion. Similar to the case of N, the implanted F also bonds to one Ge and two Zn atoms. While in the F-doped system, the F-Zn bonds are about 0.40 Å longer than O-Zn bonds presenting an obvious distorted $ZnFO_3$ tetrahedron. Thus the F-doped Zn_2GeO_4 undergoes a relative larger structure distortion with an obvious increasing of the crystal cell, caused by the stronger Coulomb repulsion between the Zn and F than that of Zn and O. As listed in Table 1, it's noted that for the N/F-codoped system with extremely distorted $ZnNO_3$ and $ZnFO_3$ tetrahedrons, the lattice parameters are closer to that of single F-doped Zn_2GeO_4. So the F-doping put a critical impact on the distorted structure of Zn_2GeO_4. The similar phenomenon was also observed in N, F-doped $ZnWO_4$[54] and $SrTiO_3$[55].

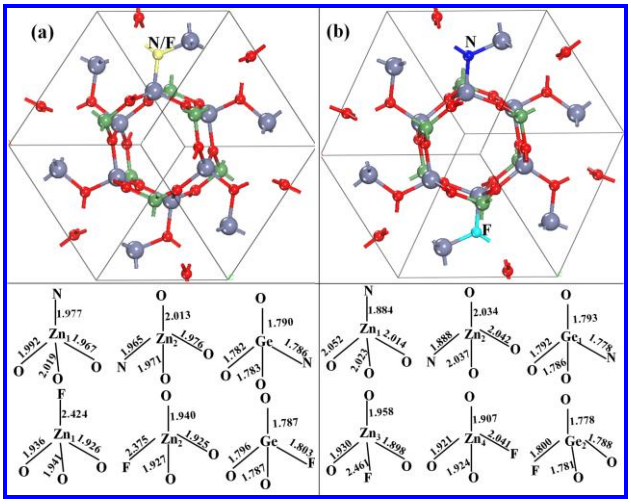

Fig. 2: The structures of (a) N or F-monodoped and (b) N/F-codoped Zn_2GeO_4 with partial bonds, the yellow ball indicates the displayed O, the blue and cyan ball are N and F atom, respectively.

Generally, the interior distorted polyhedrons constructed by different chemical bonds would induce internal dipole moment and local electrostatic field, which can promote the separation of electron-hole pairs generated by light-irradiation in a semiconductor. Here, we report the Mulliken charge population on the constitute bonds in Table 2. It's obvious that the bond lengths in the ZnO_4 and GeO_4 tetrahedrons of the pure Zn_2GeO_4 bulk are similar, and as a result the internal dipole moment is small. While in the N-doped Zn_2GeO_4 bulk, the population of N-Zn bonds (0.48 and 0.50 e) is larger than that of O-Zn bonds (0.31 to 0.39 e), suggesting the stronger interactions between N and Zn atoms than that between Zn and O. In addition, the covalent-like N-Ge bonds with the population of 0.69 e are also stronger than the Ge-O bonds. So the dipole moment of the N-doped system is enhanced because of the unbalance distribution of charges in the tetrahedron. The similar phenomenon was also observed in the F-monodoped and N/F-codoped systems, while the difference is that the F-Zn and F-Ge bonds share less charges. This is due to that the large electronegativity of F results in fewer electrons transferred from F to the adjacent Zn and Ge atoms. Presumptively, the doped systems have inequitable chemical bonds and lead to large dipole moment in the fundamental structure cells. So our results suggest that the N, F doping may create interior electrostatic field availing the separation of charge carriers.

Table 1 Lattice parameters and the calculated defect energy of Zn_2GeO_4

	a/Å	b /Å	c /Å	α /°	β /°	γ /°	E_{form} /eV
Exp[a]	8.834	8.834	8.834	107.791	107.791	107.791	–
pure	8.961	8.961	8.961	107.901	107.901	107.901	–
N-doped	8.979	8.991	8.999	107.995	107.876	107.967	-0.0495
F-doped	9.039	9.051	9.020	108.010	108.026	107.962	-5.0779
NF-codoped	9.051	9.045	9.042	108.167	108.218	108.122	-5.3677

[a]Ref. 16.

For further explore to the N, F-doping effects on the distorted geometry structure, the distributions of electrostatic potential for the pure and doped Zn_2GeO_4 are examined. As illustrated in Figure 3, it can be seen that the distributions of the electrostatic potential of N/F-codoped Zn_2GeO_4 along x, y, and z axes are distinct, which should intensify the internal field. Finally the mobility of the charge carriers

will be efficient.

Table 2 Mulliken charge population on the main bonds in the polyhedrons for the Pure and Doped systems

species	Zn1-O		Zn2-O		Zn-N	Zn-F	Ge-O		Ge-N	Ge-F
pure	0.32	0.35	0.36	0.38			0.58	0.59		
	0.37	0.38					0.61			
N-doped	0.31	0.36	0.33	0.36	0.48		0.57	0.59	0.69	
	0.37		0.39		0.50		0.60			
F-doped	0.41	0.45	0.39	0.40		0.07	0.52	0.54		0.27
			0.43				0.55			
N/F-codoped	0.28	0.30	0.40	0.41	0.69	0.07	0.35	0.44	0.76	0.29
	0.31	0.32	0.42	0.45			0.45	0.55		
	0.33		0.46	0.49			0.56	0.57		

To determine the thermodynamic stability of the doped Zn_2GeO_4, the defect formation energy, E_{form}, is calculated according to the following equations[56]:

For the N(F) single doped: $$E_{form} = E_{doped} + \mu_O - E_{undoped} - \mu_{N(F)} \quad (1)$$

For the N/F codoped: $$E_{form} = E_{doped} + 2\mu_O - E_{undoped} - \mu_N - \mu_F \quad (2)$$

where E_{doped} and $E_{undoped}$ are total energies of Zn_2GeO_4 with and without dopant(s). μ_O, μ_N, μ_F, are chemical potentials of O, N, and F, respectively, which are taken from their diatomic molecules in gas phase, i.e., μ_x = 1/2 $E_{molecule}$. The calculated results are summarized in Table 1. It is noted that the F-doping is energetically more favorable than N-doping since the E_{form} value of F-doping is much more negative than that of N-doping. The energy cost for N/F-codoping is 5.318 eV smaller than that for single N-doping, and slightly smaller than that for F-doping by 0.290 eV. Our results indicate that it's easier to incorporate N atom into the bulk in the present of F. The defect pair binding energy (E_b) is calculated to examine the coupling strength between the impurity species in the codoped Zn_2GeO_4 as following equation[57]:

$$E_b = E_{monodoped}(N@O) + E_{monodoped}(F@O) - E_{codoped} - E_{undoped} \quad (3)$$

where $E_{monodoped}$, $E_{codoped}$, and $E_{undoped}$ represent the total energy of the respective systems calculated for the same supercell size. The more positive E_b the more compatible for the defect pairs when they are present in the sample. Due to the complementary effect of charges in the neutral system, the calculated binding energies for the N, F-codoped system is 1.69 (> 0) eV, conforming that the geometry structure

with the codpoed pair is more stable than that with monodoped impurities.

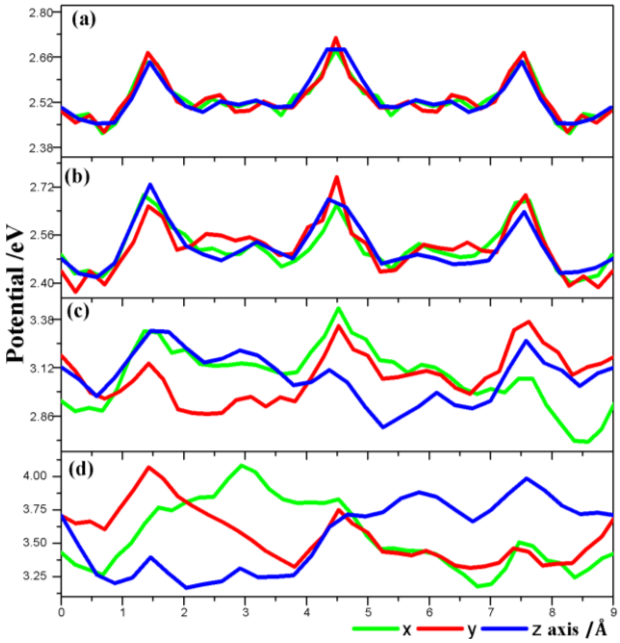

Fig. 3: The distributions of electrostatic potential for (a) pure, (b) N-doped, (c) F-doped, and (d) N/F-codoped Zn_2GeO_4 along x, y, and z axis.

3.2 Electronic Structure

In order to describe the electronic properties of Zn_2GeO_4 accurately, we first perform theoretical calculations on the pristine system with different DFT, and the corresponding results are listed in Table 3. We can see that the band gaps of 1.889, 2.005 and 3.577 eV for Zn_2GeO_4 determined by LDA, GGA and HSE06 are obviously underestimated compared with the experimental value of 4.50 eV[18, 20], while the result calculated by PBE0 (4.333 eV) is close to the experimental reports. Therefore, in the following sections, we only give the electronic properties of N, F-monodoped and N/F-codoped Zn_2GeO_4 determined by PBE0 method.

Table 3 Band gaps with different methods and effective masses of the electron (m_e^*) and the hole (m_h^*) for the pure and doped Zn_2GeO_4 at the CBM and VBM of Γ point calculated by PBE0.

systems	E_g /eV				m_e^*	m_h^*
	LDA	GGA	HSE06	PBE0		
pure	1.889	2.005	3.577	4.333	0.279	5.810
N-doped	-	-	-	3.872	0.229	1.411
F-doped	-	-	-	3.008	0.264	1.474
N/F-codoped	-	-	-	2.429	0.222	1.166

As shown in Figure 4, the pure Zn_2GeO_4 has a direct band gap with the valence band maximum (VBM) and the conduction band minimum (CBM) located at the

highly symmetrical point of Γ. In the valence band region, the flat upmost valence band is dominated by the O 2p and Zn 3d states, and the Germanium's contributions to the valence band are found in the lower energy levels. While for the conduction band, the CBM is well dispersive，which is beneficial to the mobility of the photogenerated electrons. Since the Ge 4s states are located in the bottom of the conduction band, and Zn 4s and Ge 4p states are found in the higher energy region, so the optical absorption edge of pure Zn_2GeO_4 is derived from the excitation of electrons from the O 2p to the Ge 4s states. So Ge plays an important role in the migration of interior photogenerated charges in the photocatalytic reactions. Furthermore, the calculated Mulliken charge population on the bonds are listed in Table 2, which represent the interactions between the components to a certain. According to the values for Ge-O bonds (0.58–0.61 e) of GeO_4 tetrahedrons in pure Zn_2GeO_4, we know the orbitals of Ge and O atoms sufficiently overlap with each other, indicating the covalent characteristics of Ge-O bonds. While the Zn-O bonds exhibit more ionic-bonding characteristics sharing 0.32–0.38 e between Zn and O atoms. The results of PDOS displayed in Figure 4 also confirm the above differences between Ge-O and Zn-O bonds.

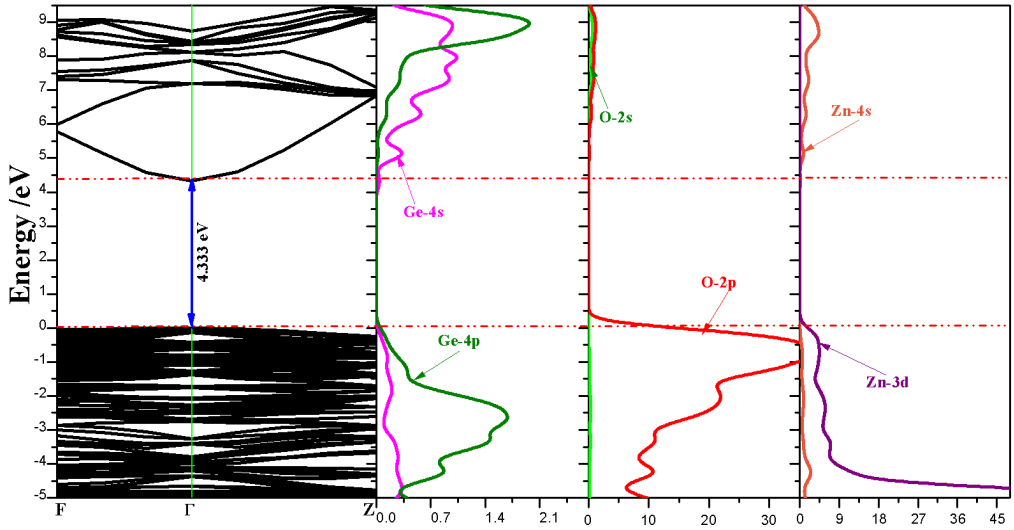

Fig. 4: Band structure and density of states plots for pure Zn_2GeO_4 calculated by PBE0. The horizontal dashed line represents the Fermi level.

In the N-doped case, due to an unpaired electron derived from nitrogen atom, the band structure is divided into spin-up and spin-down states as shown in Figure 5. For the spin-up states, the band gap of N-doped system is 4.115 eV which reveals slightly

narrower relative to the pure Zn_2GeO_4. Because of the single electronic spin in N atom, the electronic states in the spin down channel have great differences with that in spin-up channel. Since each doping N atom has one less electron than that of the substituted O atom, there is an unoccupied dopant-induced states below the CBM, which is also observed in N-doped TiO_2[58-60] $NaTaO_3$[61], and $SrTiO_3$[62]. And a localized impurity level is observed above the VBM in the N-doped Zn_2GeO_4, also reported in N-doped TiO_2[63, 64]. Thanks to these localized impurity levels acting as the frontier orbital levels, the effective band gap from the highest occupied level to the lowest unoccupied level drops to 3.872 eV, which may reduce the transition energy of the charges from the valence band to the conduction band. On the other hand, the shallow impurity bands between the VBM and CBM may act as the springboards for charge carriers. Thus, it is likely to accelerate the charge transfer between the substrate and adsorbate, which may improve the photocatalytic performances of Zn_2GeO_4. In addition, relative to the intact system, the more dispersive valence band edge is also beneficial to the mobility of the charges.

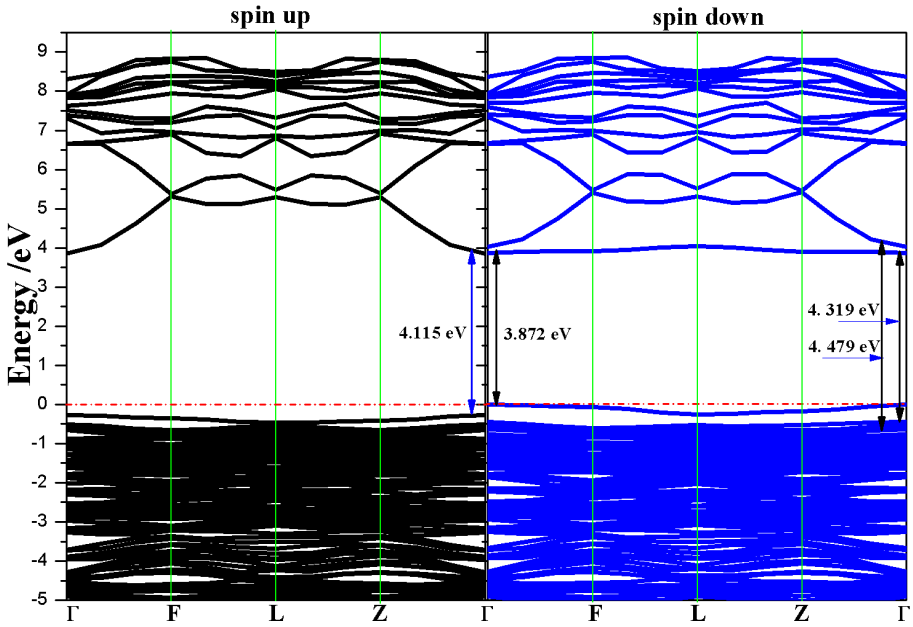

Fig. 5: Band structures of the N-monodoped Zn_2GeO_4 divided into spin-up and spin-down states. The horizontal dashed line represents the Fermi Level.

Correspondingly, the PDOS presented in Figure 6 shows that the valence band of N-doped Zn_2GeO_4 is major composed by O 2p, and Zn 3d states. The localized impurity level around the Fermi energy is originated from N 2p mixing with minor O

2p states. The lowest unoccupied states close to the CBM is dominated by spin-down N 2p and Ge 4p states. In addition, the Mulliken charges population on the N-Ge bond (0.69 e) in Table 2 shows a stronger covalent bonding character, which is larger than that on O-Ge bonds (0.57–0.60 e).

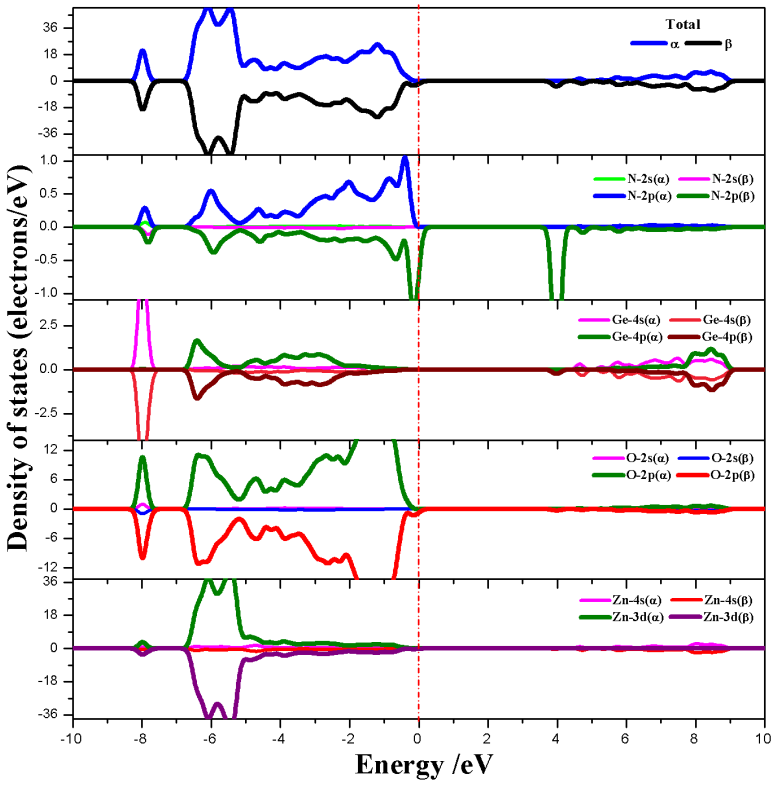

Fig. 6: Total density of states (DOS) and projected density of states (PDOS) for the substitutional N to O doped Zn_2GeO_4. The vertical dashed line indicates the Fermi Level.

Figure 7 gives the band structure of F-doped Zn_2GeO_4. Compared with the pure phase, F doping hardly put any effects on the flat and constrictive valence band, and the calculated band gap for spin-down state is 4.295 eV with negligible shrinks. The bottom of the conduction band in the spin-up channel shows more dispersive structure. As we all know, the more dispersive band results in the higher transfer rate of the charge carries. Since the valence cell of F ($2s^2 2p^5$) contains one more electron than that of O ($2s^2 2p^4$), the F-doped Zn_2GeO_4 is a electron-rich system, and the fact that the Fermi level is pinned in the CBM means the formation of some donor levels. Conspicuously, with the dispersive conduction band edge the band gap is narrowed to 3.01 eV in the spin-up states, which will extend the adsorption spectrum.

The calculated DOS for the substitution F-doped Zn_2GeO_4 in Figure 8 shows that the electronic states shifts to the lower energy obviously. The further PDOS analyses

show that most of the F 2p states is located at lower energies region of the valence band, and no F 2p states are found in the gap. This is different from the N-doped Zn_2GeO_4 as the F's 2p orbital energy lower than N's and O's [39]. Furthermore, some Ge 4s states and Zn 4s states appear at the CBM in the spin-up channels indicates the formation of the reduced metal centers by the extra electron from F similar to F-doped TiO_2[65] with reduced Ti^{3+}.

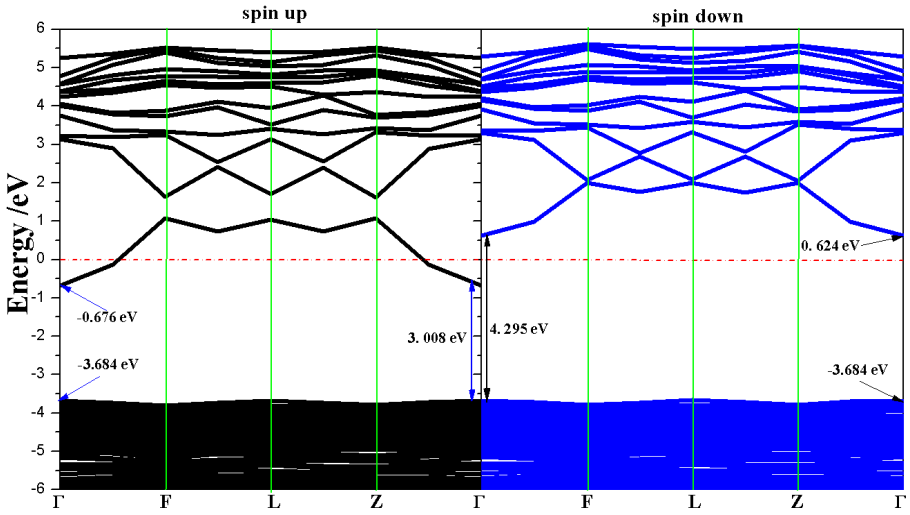

Fig. 7: Band structures of the F-monodoped Zn_2GeO_4 divided into spin-up and spin-down states. The horizontal dashed line indicates the Fermi Level.

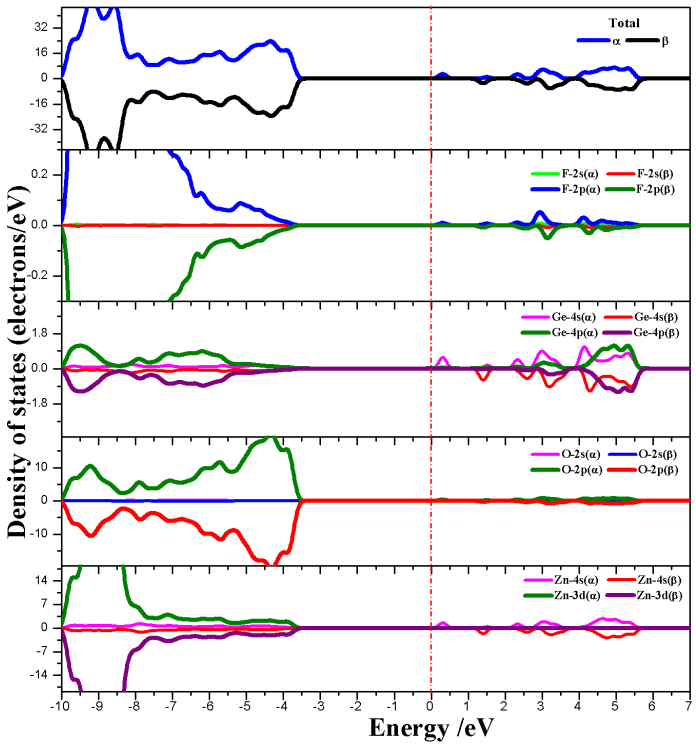

Fig. 8: Total density of states (DOS) and projected density of states (PDOS) for the substitutional F to O doped Zn_2GeO_4. The vertical dashed line indicates the Fermi Level.

For the N/F-codoped Zn_2GeO_4, the spin polarization phenomenon is not observed from the band structure as shown in Figure 9. And one cannot see the unoccupied level below the conduction band of the electron-deficiency system induced by N monodoping. Unlike the F-doped case, due to the compensation effects from the donor-accepter pair of N-F, the Fermi level is located above the VBM. The similar case have been found in the N/F-codoped TiO_2[66], $SrTiO_3$[55], and $ZnWO_4$[54]**.** Also, three localized impurity levels located below the Fermi level extend the valence band edge, and then the energy gap between the upmost valence band level and the CBM is 2.429 eV, that is to say the energy of the electronic transitions from the valence band to the conduction band greatly decreased.

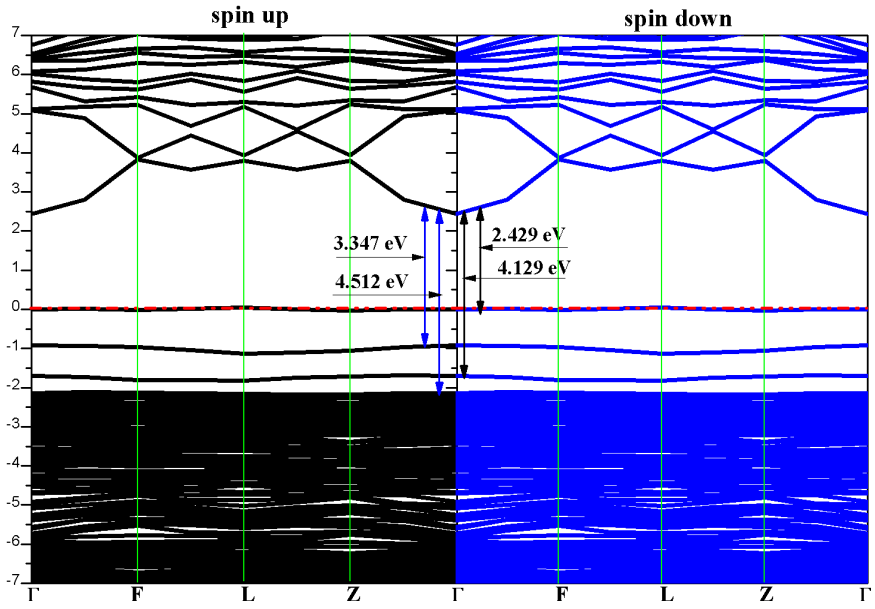

Fig. 9: Band structures of the N/F-codoped Zn_2GeO_4 without spin polarization between spin-up and spin-down states. The horizontal dash-dot red line represents the Fermi Level.

According to the DOS of the N/F-codoped Zn_2GeO_4 in Figure 10, we can see that the electronic structure of the codoped system is not a simple superposition by the N-, and F-monodoped compounds. The corresponding PDOS shows that the N 2p and F 2p states mix with O 2p states in the whole valence band. The VBM is mainly composed by the N 2p and O 2p states due to the lower energy of F 2p states. And the highest localized level around the Fermi level originated from the N 2p states hybridizing with minor Ge 4p states should act as a springboard for the excitation of electrons from the valence band to the conduction band. Consistently, in the previous

investigations on N/F-codoped TiO_2[67, 68] argued that the photocatalytic activity of N-doped TiO_2 under visible light results from narrowed band gap due to sufficient overlapping between N 2p and O 2p when the N concentration is relatively high, while at relatively low N concentration, N gives rise to isolated N 2p just above the top of the VB with little tune on the band gap[25, 68]. So, in the range of regulation, the higher the N concentration the better the band gap-narrowing effect gains. As there are some consistence between the N/F-doped Zn_2GeO_4 and N/F-doped TiO_2 with low doping concentration, we predict that with the increasing N and F concentration, and the electronic structure will be further affected significantly.

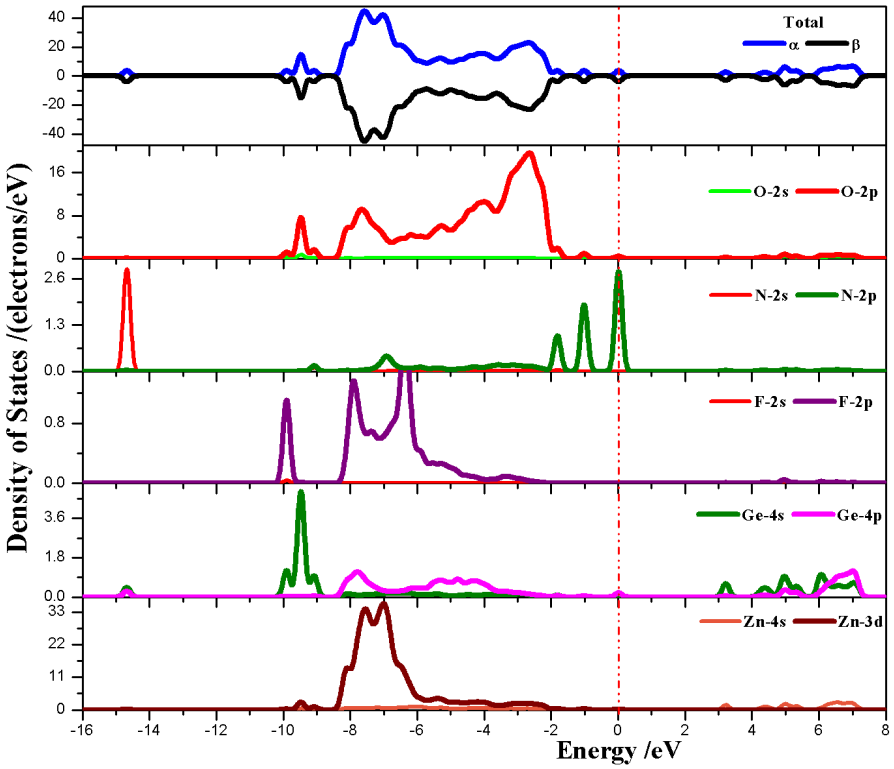

Fig. 10: Total density of states (DOS) and projected density of states (PDOS) for the substitutional N/F-codoped Zn_2GeO_4. The verticla dotted line represents the Fermi Level.

3.3 Effective Mass of Photogenerated Electrons and Holes

To shed the mobility rate of the electron hole pairs which is an important factor for the photocatalytic activity of a semiconductor [69], we compute the relative effective masse of the electron and hole in the pure and doped Zn_2GeO_4 crystals by the following formula[70], which has been widely employed in other semiconductors, such as $BiVO_4$[71], Ag_3PO_4[72], $SrNbO_3$[73], $Cu_2(OH)PO_4$[74]:

$$m^* = \frac{\hbar}{2a} \qquad (4)$$

where m^* is the effective mass of charge carriers in the unit of free-electron mass (m_e) and a is the coefficient of the second-order term in a quadratic fit of E(k) curves for the band edge corresponding to the wave vector k. And the calculated effective mass of electrons and holes are listed in Table 3. The m_e^* values of the pure and N, F-doped Zn_2GeO_4 (0.279−0.229 m_e) are much smaller than that of TiO_2 (about 1 m_e)[48], indicating that the electronic transfer in Zn_2GeO_4 bulk is more rapidly. While because of the large value of m_h^*(5.810 m_h), the transfer efficiency of holes in pure Zn_2GeO_4 is extremely low, as deduced by the less dispersive VBM structure. With N, F doping, the effective mass of holes (1.166−1.474 m_h) were lightened dramatically. So, with the modified band structure by N, F doping the mobility of photogenerated charge carriers has been improved.

3.4 Optical property

The study of the optical properties of photocatalyst is indispensible in the visible-light photocatalytic realm. We obtain the spectra within the dipole approximation by the Fermi golden rule from PBE0 wave functions. The imaginary part(ε_2) of the dielectric function due to direct interband transitions is given by the following expression[75-77]:

$$\varepsilon_2(\hbar\omega) = \frac{2e^2\pi}{\Omega\varepsilon_0}\sum_{\kappa,v,c} |\langle \psi_\kappa^c | ur | \psi_\kappa^v \rangle|^2 \delta\left(E_\kappa^c - E_\kappa^v - E\right) \qquad (5)$$

where Ω, ω , u , ν , and c are the unit-cell volume, photon frequencies, the vector defining the polarization of the incident electric field, valence bands, and conduction bands, respectively. And the real part of the dielectric function is obtained by a Kramers−Kronig transformation. The absorption coefficient $\eta(\omega)$can be obtained based on the imaginary and real part of the dielectric function[78]. The calculated optical absorption spectra for the pure and doped Zn_2GeO_4 were shown in Figure 11. Obviously, without any dopant, Zn_2GeO_4 mainly absorbs ultraviolet photon. In the N single doped Zn_2GeO_4, the visible light response has no dramatically improvements. When introducing F into the system, the absorption edge shifts to the visible-light

region. What is intriguing is that in the N/F-codoped system, the optical property shows a red-shift of about 150 nm contrasted to the spectrum of pure Zn_2GeO_4 with a sharp peak around 410 nm induced by the electronic excitation from the upmost of the valence band to the CBM. Many researchers have reported that the N/F-codoped TiO_2[39, 40, 79], $NaTaO_3$[41] with intensive response to the visible light have improved photocatalytic activity, so we think that N/F codoped Zn_2GeO_4 is also a possible candidate as an improved photocatalyst under visible light irradiation.

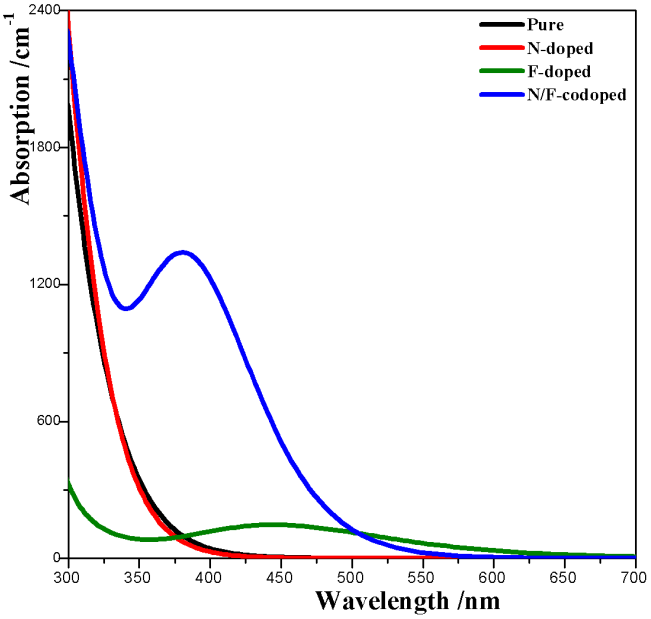

Fig. 11: Calculated total absorption coefficient spectra of pure, N-doped, F-doped, and N/F codoped Zn_2GeO_4 based on the PBE0 method.

4. Conclusions

The electronic properties of pure, N-doped, F-doped, and N/F-codoped Zn_2GeO_4 have been investigated based on DFT method. The defect formation energy values from our calculations suggest the monodoping N into Zn_2GeO_4 is difficult, while in the presence of F the incorporating of N is found to be more feasible. The smaller effective mass of holes in the N-doped system indicate the transition of the charge carrier will be more rapid. It's obviously that F doping play some roles in narrowing the band gap and induces a significant extension of the optical absorption curve. According to the electronic structure of the N/F-codoped system, the N 2p states are located just above the valence band, and the valence band edge seems more dispersive

which is convenient for the electronic transfer from VBM to CBM. So the band gap in the N/F-codoped system narrowed down to 2.429 eV, which results in a 150 nm redshift in the optical absorption spectrum with a remarkable response to the visible light. Obviously, the synergistic effects of N/F-codoping will modulate the electronic structure and optical properties of Zn_2GeO_4. Based on these results, we propose that N and F should be "good pair" for element doping into Zn_2GeO_4 to improve the photocatalytic activity under ideal visible light irradiation.

Acknowledgement

This work was supported by the National Natural Science Foundation of China (grant nos. 21171039 and 21373048), the Open Foundation of Key Laboratory for High-Energy Laser Science of the China Academy of Engineering Physics (grant no. 2012HCF05), and the Fund of Key Laboratory of Optoelectronic Materials Chemistry and Physics, Chinese Academy of Sciences (2008DP173016).

References

1 K. Maeda, K. Teramura, D. Lu, T. Takata, N. Saito, Y. Inoue, and K. Domen, *Nature*, 2006, **440**, 295-295.

2 J. Graham, and N. Hammer, Photocatalytic Water Splitting and Carbon Dioxide Reduction, Handbook of Climate Change Mitigation, Springer US, Mississippi, Oxford, MS, USA, 2012, 1755-1780.

3 N. Serpone, and A.V. Emeline, *J. Phys. Chem. Lett.*, 2012, **3**, 673-677.

4 S.N. Habisreutinger, L.S. Mende, and J.K. Stolarczyk, *Angew. Chem. Int. Ed.*, 2013, **52**, 7372-7408.

5 W.J. Yin, H.W. Tang, S.H. Wei, A. Jassim, M. Mowafak, T. John, and Y. Yan, *Phys. Rev. B*, 2010, **82**, 045106.

6 N. Wu, J. Wang, D.N. Tafen, H. Wang, J.G. Zheng, P.L. James, X. Liu, S.S. Leonard, and A. Manivannan, *J. Am. Chem. Soc.*, 2010, **132**, 6679-6685.

7 X. Wang, K. Maeda, X. Chen, K. Takanabe, K. Domen, Y. Hou, X. Fu, and M. Antonietti, *J. Am. Chem. Soc.*, 2009, **131**, 1680–1681.

8 J. Yu, W. Wang, B. Cheng, and B. Su, *J. Phys. Chem. C*, 2009, **113**, 6743-6750.

9 A. Kudo, H. Kato, and N. Seira, *J. Phys. Chem. B*, 2000, **104**, 571-575.

10 J. Sato, N. Saito, H. Nishiyama, and Y. Inoue, *J. Photoch. Photobi. A.*, 2002, **148**, 85-89.

11 H. Sun, W. Fan, Y. Li, X. Cheng, P. Li, and X. Zhao, *J. Phys. Chem. C*, 2010, **114**, 3028-3036.

12 K. Maeda, K. Teramura, N. Saito, Y. Inoue, H. Kobayashi, and K. Domen, *Pure Appl. Chem.*, 2006, **78**, 2267–2276.

13 V.B. Ram Boppana, D.J. Doren, and R.F. Lobo, *J. Mater. Chem.*, 2010, **20**, 9787.

14 W.F. Zhang, J. Tang, and J. Ye, *Chem. Phys. Lett.*, 2006, **418**, 174-178.

15 X. Lin, F. Huang, W. Wang, Y. Wang, Y. Xia, and J. Shi, *Appl. Catal. A: Gene.*, 2006, **313**, 218-223.

16 J. Sato, H. Kobayashi, K. Ikarashi, N. Saito, H. Nishiyama, and Y. Inoue, *J. Phys. Chem. B*, 2004, **108**, 4369-4375.

17 B.J. Ma, F.Y. Wen, H.F. Jiang, J.H. Yang, P.L. Ying, and C. Li, *Catal. Lett.*, 2009, **134**, 78-86.

18 Q. Liu, Y. Zhou, J. Kou, X. Chen, Z. Tian, J. Gao, S.C. Yan, and Z.G. Zou, *J. Am. Chem. Soc.*, 2010, **132**, 14385-14387.

19 X. Li, S. Ouyang, K. Naoki, and J. Ye, *Appl. Catal. A: Gene.*, 2008, **334**, 51-58.

20 S. Yan, L. Wan, Z. Li, and Z. Zou, *Chem Commun (Camb)*, 2011, **47**, 5632-56234.

21 X.B. Chen, and S. Mao, S *Chem. Rev.*, 2007, **107**, 2891-2959.

22 T. L.Thompson, and J. John T. Yates, *Chem. Rev.*, 2006, **106**, 4428-4453.

23 C.B. Mendive, D. Hansmann, T. Bredow, and D. Bahnemann, *J. Phys. Chem. C*, 2011, **115**, 19676-19685.

24 R. Asahi, T. Morikawa, T. Ohwaki, K. Aoki, and Y. Taga, *Science*, 2001, **293**, 269-271.

25 K.S. Yang, Y. Dai, and B.B. Huang, *J. Phys. Chem. C*, 2007, **111**, 12086-12090.

26 S. Tosoni, D. Fernandez Hevia, Ó. Gonz âlez D áz, and F. Illas, *J. Phys. Chem. Lett.*, 2012, **3**, 2269-2274.

27 T. Yamaki, T. Umebayashi, T. Sumita, S. Yamamoto, M. Maekawa, A. Kawasuso, and H. Itoh, *Nucl. Instr. and Meth. in Phys. Res. B*, 2003, **206**, 254-258.

28 R. Shi, G.L. Huang, J. Lin, and Y. Zhu, *J. Phys. Chem. C*, 2009, **113** 19633-19638.

29 H. Jiang, H. Dai, J. Deng, Y. Liu, L. Zhang, and K. Ji, *Solid State Sci.*, 2013, **17**, 21-27.

30 R. Long, and N.J. English, *Chem. Phys. Lett.*, 2010, **498**, 338-344.

31 H. Sun, W. Fan, Y. Li, X. Cheng, P. Li, and X. Zhao, *J. Solid State Chem.*, 2010, **183**, 3052-3057.

32 J. Xu, S. Huang, and Z. Wang, *Solid State Commun.*, 2009, **149**, 527-531.

33 W.J. Yin, H. Tang, S.H. Wei, Al Jassim, M. M., J. Turner, and Y. Yan, *Phys. Rev. B*, 2010, **82**, 045106.

34 M. Niu, W. Xu, X. Shao, and D. Cheng, *Appl. Phys. Lett.*, 2011, **99**, 203111.

35 W. Zhu, X. Qiu, V. Iancu, X.-Q. Chen, H. Pan, W. Wang, N. Dimitrijevic, T. Rajh, H. Meyer, M. Paranthaman, G. Stocks, H. Weitering, B. Gu, G. Eres, and Z. Zhang, *Phys. Rev. Lett.*, 2009, **103**, 2264011-2264014.

36 R. Long, and N.J. English, *Appl. Phys. Lett.*, 2009, **94**, 132102.

37 R. Long, and N.J. English, *Phys. Rev. B*, 2011, **83**.

38 M. Pelaez, A.A. de la Cruz, E. Stathatos, P. Falaras, and D.D. Dionysiou, *Catal. Today*, 2009, **144**, 19-25.

39 K. Pathakoti, S. Morrow, C. Han, M. Pelaez, X. He, D.D. Dionysiou, and H.M. Hwang, *Environ. Sci. Technol.*, 2013, **47**, 9988-9996.

40 A.E. Giannakas, E. Seristatidou, Y. Deligiannakis, and I. Konstantinou, *Appl. Catal. B: Environ.*, 2013, **132-133**, 460-468.

41 B. Modak, and S.K. Ghosh, *Chem. Phys. Lett.*, 2014, **613**, 54-58.

42 S.K. Park, T.K. Yun, and J.Y. Bae, *J. Nanosci. Nanotechnol.*, 2015, **15**, 5967-5970.

43 C.D. Valentin, E. Finazzi, G. Pacchioni, and A. Selloni, *Chem. Mater.*, 2008, **20**, 3706-3714.

44 M. Li, J. Zhang, W. Dang, S.K. Cushing, D. Guo, N. Wu, and P. Yin, *Phys. Chem. Chem. Phys.*, 2013, **15**, 16220-16226.

45 K. Takanabe, T. Uzawa, X.C. Wang, K. Maeda, K. Masao, J. Kubota, A. Kudo, and K. Domen, *Dalton Trans.* , 2009, 10055-10062.

46 J.H. Huang, Y.J. Cui, and X.C. Wang, *Environ. Sci. Technol.*, 2010, **44**, 3500-3504.

47 S.J. Clark, M.D. Segall, C.J. Pickard, P.J. Hasnip, M.I.J. Probert, K. Refson, and M.C. Payne, *Z. Kristallogr.*, 2005, **220**, 567-570.

48 A. Ruzsinszky, J.P. Perdew, G.I. Csonka, O.A. Vydrov, and G.E. Scuseria, *J. Chem. Phys.*, 2006, **125**, 096105.

49 J.P. Perdew, *Phys. Rev. B*, 1981, **23**, 5048-5079.

50 B.G. Janesko, T.M. Henderson, and G.E. Scuseria, *Phys. Chem. Chem. Phys.*, 2009, **11**, 443-454.

51 C. Adamo, and V. Barone, *The Journal of Chemical Physics*, 1999, **110**, 6158-6170.

52 A. Carlo, and B. Vincenzo, *Chem. Phys. Lett.*, 1998, **298** 113-119.

53 D. Vanderbilt, *Phys. Rev. B*, 1990, **41**, 7892-7895.

54 L. Sun, X. Zhao, X.F. Cheng, H.G. Sun, Y.L. Li, P. Li, and W. Fan, *J. Phys. Chem. C*, 2011, **115**, 15516-15524.

55 W. Wei, Y. Dai, M. Guo, L. Yu, H. Jin, S. Han, and B. Huang, *Phys. Chem. Chem. Phys.*, 2010, **12**, 7612-7619.

56 C.G. Van de Walle, and J. Neugebauer, *J. Appl. Phys.*, 2004, **95**, 3851-3879.

57 Y. Gai, J. Li, S. Li, X. Bai, and S. Wei, *Phys. Rev. Lett.*, 2009, **102**, 036402.

58 R.T. Gemma, L. Torbjorn, L. Jun, G.G. Claes, and E.L. Sten, *J. Phys. Chem. B*, 2004, **108**,

5995-6003.
59 N. Serpone, *J. Phys. Chem. B*, 2006 **110**, 24287-24293.
60 C. Belver, R. Bellod, S.J. Stewart, F.G. Requejo, and M. Fernández-García, *Appl. Catal. B: Environ.*, 2006, **65**, 309-314.
61 B. Modak, K. Srinivasu, and S.K. Ghosh, *J. Phys. Chem. C*, 2014, **118**, 10711-10719.
62 B. Modak, K. Srinivasu, and S.K. Ghosh, *Phys. Chem. Chem. Phys.*, 2014, **16**, 24527-24535.
63 M. Lan, Y. Zhang, and P.N. Wang, *Chem. Phys. Lett.*, 2008, **458** 341-345.
64 H. Irie, Y. Watanabe, and K. Hashimoto, *J. Phys. Chem. B*, 2003, **107**, 5483-5486.
65 A. M. Czoska, S. Livraghi, M. Chiesa, E. Giamello, S. Agnoli, G. Granozzi, E. Finazzi, C. Di Valentin, and G. Pacchioni, *J. Phys. Chem. C*, 2008, **112** 8951-8956.
66 X. Xi, P. Dong, H. Pei, G. Hou, Q. Zhang, R. Guan, N. Xu, and Y. Wang, *Comp. Mater. Sci.*, 2014, **93**, 1-5.
67 N. Serpone, *J. Phys. Chem. B*, 2006, **110**, 24287-24293.
68 C.D. Valentin, E. Finazzi, G. Pacchioni, A. Selloni, S. Livraghi, A.M. Czoska, M.C. Paganini, and E. Giamello, *Chem. Mater.*, 2008, **20**, 3706–3714.
69 X.B. Chen, S.H. Shen, L.J. Guo, and M.S. S., *Chem. Rev.*, 2010, **110**, 6503-6570.
70 C. Letizia, J.M. García Lastra, A. Iacomino, S. Ossicini, J. Zhao, H. Petek, and A. Rubio, *Phys. Rev. B*, 2010, **82**, 045207.
71 Z. Zhao, Z. Li, and Z. Zou, *Phys. Chem. Chem. Phys.*, 2011, **13**, 4746-4753.
72 X. Ma, B. Lu, D. Li, R. Shi, C. Pan, and Y. Zhu, *J. Phys. Chem. C*, 2011, **115**, 4680-4687.
73 Y. Zhu, Y. Dai, K. Lai, Z. Li, and B. Huang, *J. Phys. Chem. C*, 2013, **117**, 5593-5598.
74 Z. Li, Y. Dai, X. Ma, Y. Zhu, and B. Huang, *Phys. Chem. Chem. Phys.*, 2014, **16**, 3267-3273.
75 A. Read, and R. Needs, *Phys. Rev. B*, 1991, **44**, 13071-13073.
76 Y.Y. Peter, Fundamentals of semiconductors, Springer, 1996.
77 G. Ghosh, Handbook of Optical Constants of Solids: Handbook of Thermo-Optic Coefficients of Optical Materials With Applications, Academic Press, 1998.
78 S. Saha, T. P. Sinha, and A. Mookerjee, *Phys. Rev. B: Condens. Matter Mater. Phys.*, 2000, **62**, 8828.
79 L. Di, H. Hajime, H. Shunichi, and O. Naoki, *Chem. Mater.*, 2005, **17**, 2596-2602.